Journal of Adhesion Science and Technology

ISSN: (Print) (Online) Journal homepage: https://www.tandfonline.com/loi/tast20

Loading-rate effect on tensile and bending strength of 3D-printed polylactic acid adhesively bonded joints

M. Gokhan Atahan & M. Kemal Apalak

To cite this article: M. Gokhan Atahan & M. Kemal Apalak (2022) Loading-rate effect on tensile and bending strength of 3D-printed polylactic acid adhesively bonded joints, Journal of Adhesion Science and Technology, 36:3, 317-344, DOI: 10.1080/01694243.2021.1922022

To link to this article: https://doi.org/10.1080/01694243.2021.1922022

JOURNAL OF ADHESION SCIENCE AND TECHNOLOGY
2022, VOL. 36, NO. 3, 317–344
https://doi.org/10.1080/01694243.2021.1922022

Loading-rate effect on tensile and bending strength of 3D-printed polylactic acid adhesively bonded joints

M. Gokhan Atahan[a] and M. Kemal Apalak[b]

[a]Department of Mechanical Engineering, Abdullah Gul University, Kayseri, Turkey; [b]Department of Mechanical Engineering, Erciyes University, Kayseri, Turkey

ABSTRACT

Additive manufacturing provides the production of many machine parts and components with complex geometries. The adhesive bonding technique can be alternative method for joining parts produced with additive manufacturing. This experimental study investigates the applicability of the adhesive bonding technique for PLA (polylactic acid) adherends produced with additive manufacturing and especially the effects of loading rate on the strength of 3D-printed PLA adhesive single-lap joints under tensile, three-point bending (with shear) and four-point bending (no shear effect) loadings. Both PLA and adhesive tensile test specimens exhibited a better strength but lower failure strain with increasing loading rate. PLA had better mechanical behaviour in the raster orientation than those in the layer-build direction. The strength of adhesive single-lap joints improved slightly with increasing loading rate for the tensile and three-point bending tests whilst a decrease of strength and an improvement of bending stiffness were observed for the four-point bending test. Failure initiated at the free edge of the top adherend-adhesive interface for all tests, and propagated along this interface for both bending tests whilst a sudden through-the-thickness failure of top adherend occurred for tensile load after a small interfacial damage propagation. The failure propagation appeared in a wavy form for the three-point bending test whilst it was along the top adherend-adhesive interface for the four-point bending test. Digital Image Correlation (DIC) method for tensile tests showed that the peeling and shear strains were more critical and concentrated around both free edges of adherend-adhesive interfaces; thus, at the right free edge of the top adherend-adhesive interface and at the left free edge of the bottom adherend-adhesive interface.

ARTICLE HISTORY
Received 12 December 2020
Revised 14 April 2021
Accepted 15 April 2021

KEYWORDS
Additive manufacturing; 3D-printing; PLA-polylactic acid; three-point bending; four-point bending; adhesive bonding; single-lap joint

1. Introduction

Additive manufacturing is a production system based on modelling three-dimensional parts with complex geometries in a computer program and printing materials in layers

CONTACT M. Kemal Apalak apalakmk@erciyes.edu.tr Department of Mechanical Engineering, Erciyes University, Kayseri, Turkey

by using 3D-printers. Advantages, such as easy-use of 3D-printers, dimensional tolerance sensitivity, increasing material diversity with developing technology, have led industrial applications to additive manufacturing technology. The mechanical characterization of materials produced with additive manufacturing using fused deposition modelling (FDM) method and the effects of printing speed, build orientation, raster angle and layer thickness are being still studied [1].

Nowadays, composite materials can be produced with additive manufacturing using 3D printers. The adhesive bonding technique can be used to join various types of materials produced with the additive manufacturing, such as polymer, composite, metal. However, the usability of fused deposition molding manufacturing technique with polymeric materials and structural adhesives, and the enhanced adhesive bonding strength require a detailed investigation. Mechanical strength tests, such as tensile and bending tests, provide useful information about the overall mechanical response of adhesively bonded joints. Single-lap joint offers simplicity to characterize adhesive strength, and is used widely for testing purposes [2,3].

Grant et al. [4] tested adhesively bonded joints under a tensile load (only shear), a four-point loading (pure bending) and a three-point loading (bending with shear). They investigated the effects of overlap length, bond-line thickness, and spew fillet on the bond strength by using a toughened epoxy-based adhesive and mild steel adherends. The three-point bending and tension loadings had similar effects on the adhesive strength whilst the four-point bending test did not cause any failure as the steel adherend underwent yielding before the joint failure.

Esmaeili et al. [5] showed that embedding metal fibres into the adhesive layer had a significant effect of improving the bending load capacity of the adhesive single-lap joint, and the maximum normal stresses in the adhesive layer could be relieved; consequently, the load bearing capability of the adhesive joint could be improved by reducing the distance between fibres, increasing the fibre diameter and selecting a stiffer material in the longitudinal direction. Karachalios et al. [6] showed that increasing adherend thickness improved the bending behaviour of the adhesive single-lap joint whereas the overlap length had a negligible effect relying on the four-point bending tests of adhesive single-lap joints having hard steel adherends bonded by a structural epoxy adhesive.

Malvade et al. [7] determined the non-linear mechanical behaviours of adhesively bonded double lap shear joints for various extension rates and temperatures. They showed that at a low temperature both von Mises and exponent Drucker-Prager criteria exhibited compatibility with experimental load-extension curves while at a high temperature von Mises condition tended to yield an apparent softer joint behaviour, while only the use of an exponent Drucker-Prager criterion gave much closer load-displacement curves to the experimental ones. Blackman et al. [8] investigated the effects of test rate and the mode of loading on the fracture energy of adhesively-bonded fibre-composite joints composed of various carbon-fibre reinforced-polymer matrix composite substrates and two different types of structural epoxy-adhesives. They observed various different fracture paths which were either cohesive, in the adhesive layer, or interlaminar in the composite substrates. They indicated that an exact fracture path

was dependent on the type of composite substrate and adhesive, the loading mode, but the nature of the fracture path was quite insensitive to the test rate.

Al-Zubaidy et al. [9] examined the effect of loading rate on the adhesion bond between carbon fibre reinforced polymer (CFRP) sheets and steel under various dynamic loading rates by utilising pull-off tests. They reported that the loading speed had an improving effect on the evaluated bond strength of adhesion between CFRP sheets and steel for both types of CFRP/steel samples with one and three CFRP layers of both Araldite 420 and MBrace saturant adhesives, the loading rate affected the failure mode of samples with one CFRP layer for both Araldite 420 and MBrace saturant adhesives, and the increase in pull-off strength was about 100% on average within the dynamic test loading rates. Al-Zubaidy et al. [10] also showed that the mechanical properties of unidirectional CFRP (CF130) and Araldite 420 and MBrace saturant adhesives at quasi-static and various cross-head stroke rates were strain rate-dependent and the failure patterns of CFRP and both adhesives changed apparently.

Murakami et al. [11] investigated the influence of loading rates and the combined stress states of tension and shearing on the strength, strain, and absorbed energy of adhesively bonded cylindrical butt joint specimens under quasi-static (6.67×10^{-2} MPa/s) and high-rate (10^3 MPa/s) loading conditions. They observed that the fractured surfaces were not affected by the loading rates in the combined loading tests and adhesive failure predominantly occurred in the ductile adhesive when the ratio of shear loading was high, the joint strength under high-rate loading was greater than that under quasi-static loading for both the ductile and brittle adhesives, the strength parameters depended on the rates, and the failure strain and absorbed energy of the brittle adhesive were slightly dependent on the strain rate.

However, a limited number of studies are available on the tensile and bending strengths of 3D-printed adhesively bonded joints. Kovan et al. [12] experimentally examined the effects of layer thickness and printing orientation on the bond strength of the parts which were produced in three different printing orientations and different layer thicknesses by additive manufacturing. The layer thickness and printing orientation were found to influence the adhesion strength. Thus, the edgewise printing orientation provided the highest adhesion strength with a less layer thickness whereas the flat-wise printing orientation achieved the highest adhesion strength with a higher layer thickness. Garcia and Prabhakar [13] applied the polymer additive manufacturing technology for imparting texture to bond regions in adhesively bonded joints. They improved apparently the shear strength of adhesively bonded single lap joints by fusing structural reinforcements to adherends. They compared the peak loads, shear stresses and failure types of pure adhesive joints and 3D-printed adhesive joints for four different texture geometries. Pure adhesive joints failed adhesively at low peak loads and shear strength while 3D-printed adhesive joints failed at higher average peak loads and shear strengths with predominantly cohesive failure.

Spaggiari and Denti [14] investigated the combined usability of fused deposition molding manufacturing technique with polymeric materials and structural adhesives, and attempted to enhance the adhesive performance using single lap joints with two adhesives and seven different surface morphologies. The adhesive bonding did not diminish the load carrying capacity and stiffness of joints and improved slightly the

peak force. In addition, the surface morphology was reported to have a negligible effect on the performance of the adhesive joints since a weak mechanical interlocking of the parts occurred due to peel stresses and the predominant effect of stress concentrations at the corners, which are main reason of substrate failure. Bürenhaus et al. [15] investigated the influence of the adhesive type, the surface character of the parts which were produced by the additive manufacturing process and the design of the bond area on the bond strength. They used the parts made of ULTEM 9085 and six different adhesives (acrylate resin, polyurethane adhesive, and epoxy resins) and studied their compatibility with the ULTEM 9085 parts, the influence of different pretreatments (mechanical roughening, plasma activation), and different surface structures with different surface character. They indicated that the maximum lap shear strength could be achieved by using two-component epoxy resins and the adhesion between the ULTEM 9085 and the polyurethane was insufficient. An improving effect of the plasma treatment was determined only for the combination of ULTEM 9085 with the polyurethane adhesive whilst the scarf and finger joints reflected the best results.

Caminero et al. [16] evaluated the effects of layer thickness and fibre volume content on the interlaminar bonding performance of 3D printed continuous carbon, glass and Kevlar fibre reinforced nylon composites produced by the fused deposition modelling technique. They indicated that the shear strength of 3D-printed composites was considerably improved in comparison with those of common prepreg materials. Leicht et al. [17] determined the tensile strength of adhesive bonds by using three different epoxy resins and laser sintered polyamide 12 by means of additive manufacturing. They showed that the adhesion strength can be improved by using various methods, such as post-treatment by chemical smoothing or pre-treatment by atmospheric pressure plasma. Yap et al. [18] compared the adhesive strengths of two commercial adhesives, epoxy and cyanoacrylate (CA), on 3D printed plastic materials, Acrylonitrile Styrene Acrylate (ASA) and Nylon 12 Carbon Fibre (NCF) and determined the adhesive properties of the single lap shear test specimens with and without post-curing at elevated temperature. They also compared the strength of single-lap specimens as one piece produced with a 3D printer with the bonding performances of both adhesives. In case of ASA and NCF, the adhesive strength for CA was much higher than that of epoxy. Thus, ASA and NCF bonded with CA had average failure loads whereas those bonded with epoxy had significantly lower failure loads. Both heat and surface treatments improved the adhesive strength of epoxy with both adherend materials, but this improved adhesive strength of epoxy was still significantly weaker than that of CA.

The present studies on the adhesively bonded joints having 3D-printed parts are limited, and concentrate on the determination of the mechanical properties of materials produced with additive manufacturing under different test conditions. This study investigates the applicability of adhesive bonding technique to join 3D-printed polylactic acid (PLA) adherends produced by additive manufacturing and the effect of the loading rate on both tensile and bending strengths of 3D-printed PLA adhesive single-lap joints. For this purpose, the tensile behaviours of adhesive and PLA specimens, the tensile, bending strengths of 3D-printed polylactic acid adhesive single-lap joints were experimentally investigated by means of tensile, three-point bending (with shear) and four-point bending tests.

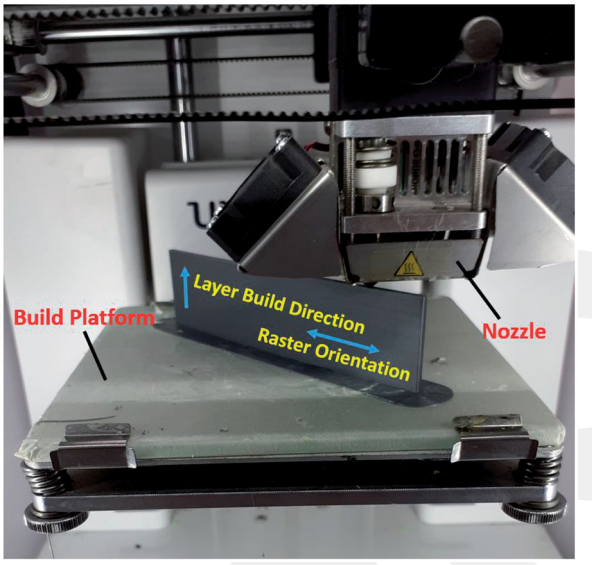

Figure 1. Production of 3D printed-PLA tensile test specimen and adherend.

2. Experimental

2.1. Sample preparation

In order to determine the effect of loading rate (cross-head speed) on the strength of adhesively bonded 3D-printed polylactic acid single-lap joints an experimental study was carried out. First, the uni-axial mechanical behaviours of both PLA and Araldite 2015 adhesive specimens were determined.

Two types of PLA dogbone specimens for tensile test were produced with Fused Deposition Modelling (FDM) method (Figures 1 and 2(b)). The first type of PLA dogbone specimen has a raster orientation coinciding with the line of action of applied axial load and the second type of PLA dogbone specimen has a layer-build direction coinciding with the line of action of applied axial load. An additional machining operation was not fulfilled for these specimens. PLA specimens were prepared and tested in accordance with ASTM D638-14 standard [19]. According to this standard Ayatollahi et al. [20] investigated the influence of in-plane raster angle on tensile and fracture strengths of 3D-printed PLA specimens, Caminero et al. [21] performed mechanical tests of additively manufactured PLA-based composites using fused filament fabrication and Ferreira et al. [22] studied mechanical characterization and micrography of 3D printed PLA and PLA reinforced with short carbon fibers.

Adhesive specimens were prepared and tested in accordance with ISO 527-1 standard [23]. A mold was designed and produced with the same method (FDM) for tensile test specimens of bulk adhesive material (Figures 2(a) and 3(a)). Araldite 2015 two-component adhesive was poured into this mold and the adhesive specimen was extracted from the mold after a suitable curing time of 24 h at room temperature.

PLA adherends of adhesive single-lap joints were produced with FDM method from PLA plastic filaments and each layer of adherend was arranged on the edge. Namely,

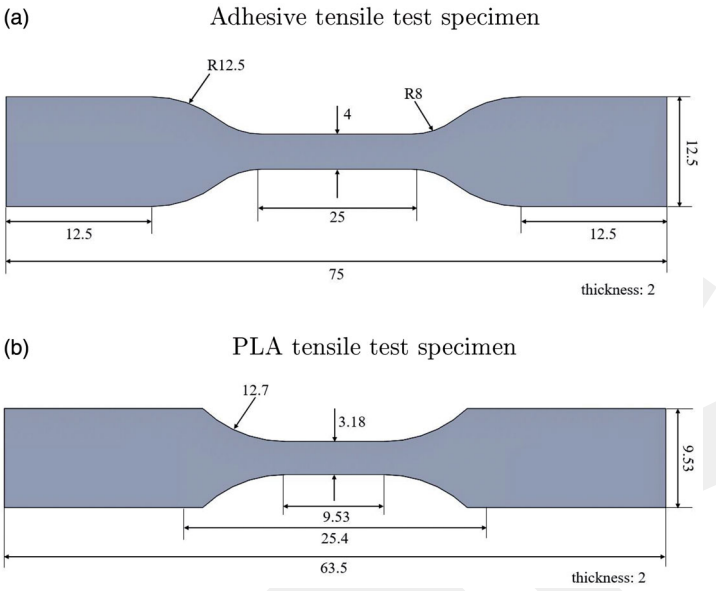

Figure 2. Dimensions of (a) adhesive and (b) PLA tensile test specimens (all dimensions in mm).

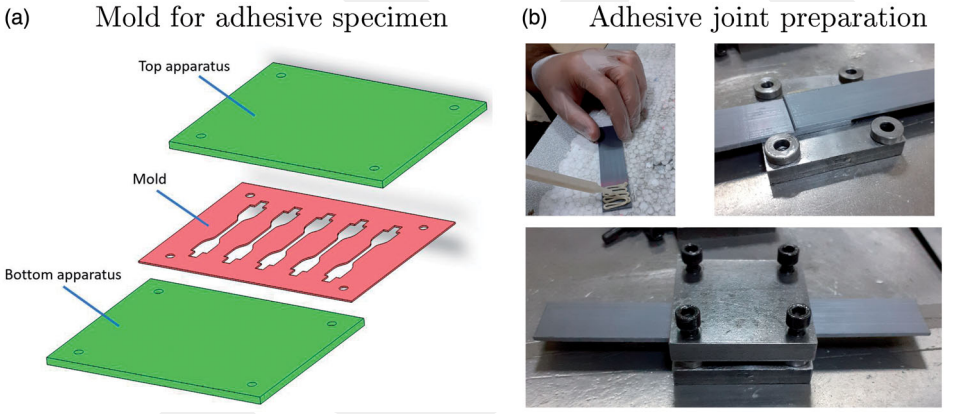

Figure 3. (a) Mold for adhesive specimen and (b) preparation of 3D-printed PLA adhesive single-lap joint.

the filament alignment raster orientation of adherends is directed along the line of action of tensile load (Figure 1). PLA adherends (Figure 4) were designed in dimensions of 25 × 100 × 2 mm using Solidworks software [24] and STL file exported for 3D printing software Cura [25]. Then, G-code files were generated by using Cura software and PLA adherends were produced layer by layer using a Ultimaker^2 Go 3D printer with PLA plastic filaments in a diameter of 2.85 mm. The process parameters of PLA adherends for the 3D printer were an infill density of 100%, a layer thickness of 0.1 mm and a feed rate of 60 mm/s. The filaments of adherends were laid in the same and perpendicular printing directions as those of the tensile specimens made of PLA material. Roughening surfaces prior to bonding can enhance the strength of adhesive

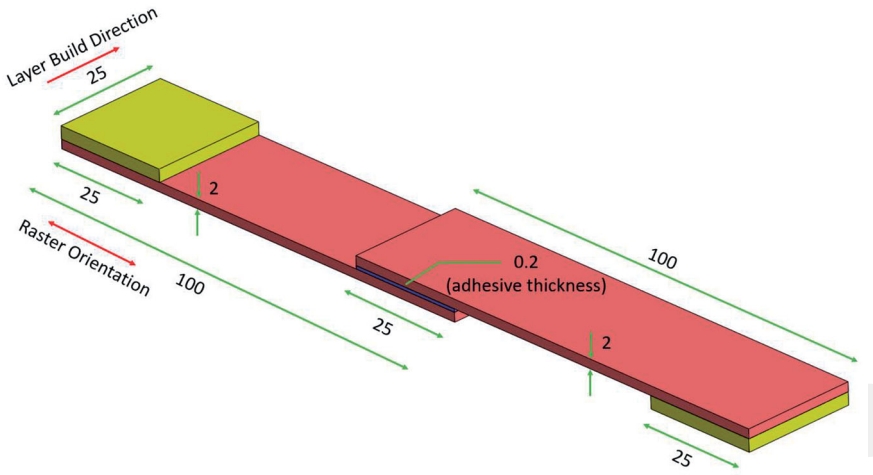

Figure 4. Structure of 3D-printed PLA adhesive single-lap joint for tensile and bending tests (all dimensions in mm).

joints. Jennings [26] discussed the effect of surface roughness of metallic adherends on the adhesive joint strength and indicated that roughening method is dependent on the material properties of adherend and adhesive. Harris and Beevers [27] indicated that although grit blasting resulted in higher adhesive joint strengths compared with the as-rolled surfaces of the substrates, there was no difference in strength between fine and coarse grits. Spaggiari and Dragoni [28] reported that the mechanical surface treatment, such as sandpapering or sandblasting of adherends made of AISI-1010 steel and aluminum 2011 enhanced the static strength of adhesive lap joints and lead to a higher probability of cohesive failure. Therefore, the surface roughness of PLA adherends was measured as $2.11 \pm 0.1 \mu m$ in the raster direction and $7.28 \pm 0.2 \mu m$ in the layer build direction by using Mitutoyo Surface Tester Instrument. Any mechanical surface treatment was not applied the bonding surfaces of PLA adherends. All stress-strain variations and joint strengths were determined based on these surface roughness values for tensile and flexural loads. Adhesively bonded 3D-printed PLA single-lap joints (Figures 3(b) and 4) were produced in dimensions as specified in ASTM D5868-01 [29]. The testing standard ASTM D5573-99 covers the damage classification of fibre reinforced plastic joints and is also suitable for the testing of adhesive lap joints with PLA adherends [30]. A suitable curing of 24 h at least was applied to adhesively bonded joints at room temperature.

Gleich et al. [31] pointed out a theoretical optimum bondline thickness (0.1–0.5 mm) and the importance of using interface stresses in failure criteria or strength analysis of bonded joints whether bonded joints are manufactured well or poorly. Kawashita et al. [32] studied the influence of adhesive bond line thickness on the adhesive fracture toughness and attempted to establish whether the peel fracture is cohesive or interfacial fracture for a number of metal toughened epoxy laminates. They indicated a relationship between toughness and bond line thickness, that the cohesive fracture can occur even when the adhesive coating thickness is small in comparison to the bond line thickness. Castagnetti et al. [33] investigated the effect of adhesive

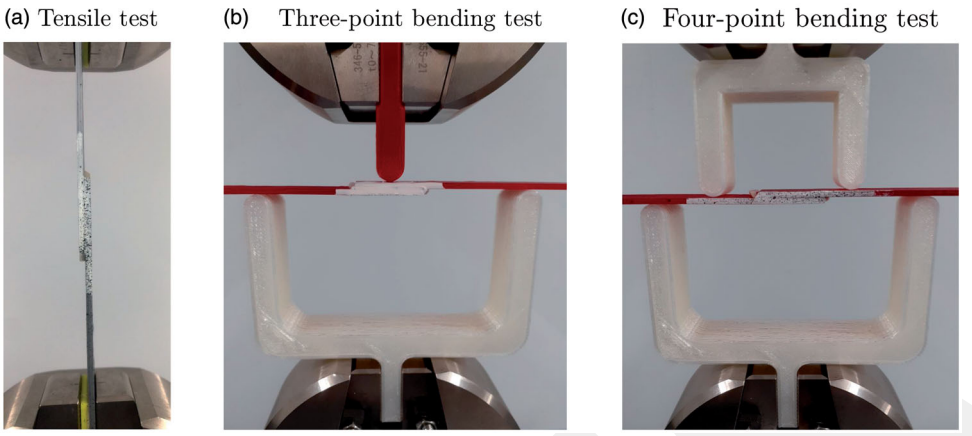

Figure 5. (a) Tensile, (b) three-point bending and (c) four-point bending test set-ups.

thickness (0.05–0.5 mm) on the static shear strength of two adhesives in a tubular lap joint, and reported that the static shear strength increased with decreasing adhesive thickness for a modified methacrylate (Multibond 330) resulting in a cohesive failure, but the adhesive shear strength was independent of the adhesive thickness for a high strength epoxy (Hysol 9514) which fails very close to the interface. Akhavan-Safar et al. [34] studied the effect of bondline thickness (0.1–0.5 mm) on the strength of adhesive single lap joints by considering longitudinal strains at critical distances from the adhesive free edges along the adhesive mid-plane and remarked that they increased with decreasing adhesive thickness, and this method was capable of considering the experimental strength reduction with increasing adhesive thickness. Consequently, the adhesive thickness was kept constant at 0.2 mm as possible with the bonding set-up (Figure 3(b)). Four washers of 4.2 mm thickness between the male and female parts of apparatus were located to adjust this adhesive thickness. After joining adhesive thickness was measured as 0.2 ± 0.02 mm. The bonding surfaces of both adherends were cleaned using ethanol, and adhesive bonding process were applied according to the manufacturer's recommendations.

2.2. Mechanical properties and testing

The tensile tests of PLA specimen, adhesive specimen were carried out at five different loading rates (cross-head speeds) of 1, 10, 20, 30 and 50 mm/min *via* Shimadzu tensile test machine. The tensile test of adhesive specimen was performed according to ISO 527-2 [23] test standard (Figure 2(a)), and PLA specimen was tested in tension according to the ASTM D638-14 (Type V) [19] test standard (Figure 2(b)). The testing standards ISO 527-2 and ASTM D638-14 recommend the determination of modulus of elasticity for adhesive and PLA specimens at a cross-head speed of 1 mm/min, and it should be constant for higher strain rates. Machado et al. [35] considered that the elastic moduli and the mode I and mode II fracture energy were not strain rate dependent while fracture toughness is negligibly strain rate dependent since drastic changes were not observed. The adhesively bonded single-lap joints were also tested in tension at

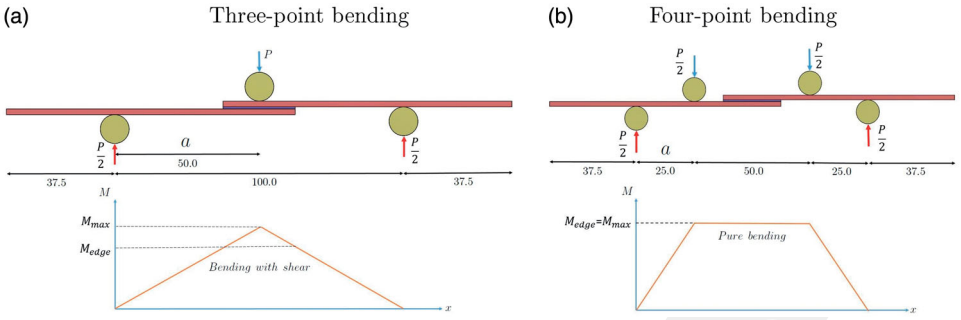

Figure 6. Dimensions, loading conditions and bending moment diagrams of 3D-printed PLA adhesive single-lap joint for (a) three-point, (b) four-point bending tests (all dimensions in mm).

four loading rates of 1, 10, 20, and 50 mm/min (Figure 5(a)). The tensile tests of adhesive, PLA specimens and the adhesively bonded single-lap joints were repeated five times for each loading rate. The method of least-squares (regression analysis) was applied to five data sets for each loading rate to approximate a stress-strain curve.

The bending stiffness and strength of adhesively bonded 3D-printed PLA single-lap joints can be evaluated by both three-point bending and four-point bending tests (Figure 5(b,c)). Additively-manufactured plastic tools, such as support, mold and indenter, by fused deposition modelling method have been used successfully for sheet metal forming processes with high precision [36–38]. Thus, polylactic acid offers a high elasticity modulus (1.9–2.4 GPa) and yield stress (22 MPa) which are about 1/100 and 1/10 of steel, respectively [39]. The span between two suports is not short. Therefore, 3D-printed tools made of polylactic acid can be used successfully for bending tests without causing compliance effects. The three-point bending test creates a linearly increasing/decreasing bending moment and a constant transverse shear force through the overlap region (Figures 6(a)); therefore, it is possible to consider the effects of both bending moment and transverse shear force. The four-point bending test allows only a constant bending moment through the bonding region whilst the shear force is zero (Figures 6(b)).

The three-point and four-point bending tests were performed at the loading rates of 1, 10, 30, 50 mm/min, respectively. PLA material exhibits partially similar mechanical behaviours to those of unreinforced plastics. The flexural properties of the unreinforced plastics can be determined according to ASTM D790-17 for three-point bending test and ASTM D6272-17 for the four-point bending test [40,41]. Based on these test standards the specimen dimensions as well as the load and support locations were designated (Figure 6). Thus, the three-point bending test requires a distance of 100 mm between two supports and a central concentrated load applied at a distance of 50 mm from each support. The four-point bending test requires a distance of 100 mm between two supports and a half concentrated load applied at two locations at a distance of 50 mm from each support.

Grant et al. proposed a simple method for calculating the bending moments in the three and four-point bending tests [4]. For a three-point bending test (Figure 6(a)), the

maximum bending moment occurs at the midpoint of the adhesive single-lap joint as follows:

$$M_{max} = \frac{P}{2}a \tag{1}$$

where P is applied load and a indicates distance between the load and support positions. The bending moment at the free edges of the overlap region becomes:

$$M_{edge} = M_{max}\left(a - \frac{l}{2}\right)\frac{1}{a} \tag{2}$$

where l is distance between two supports. For a four-point bending test of an adhesive single-lap joint (Figure 6(b)) the bending moment through the overlap region is constant as follows:

$$M_{edge} = M_{max} = \frac{P}{2}a \tag{3}$$

The distance a between the load and support positions is different for each of three- and four-bending tests (Figure 6); therefore, the corresponding maximum M_{max} and edge M_{edge} moments are also different (Equations 1–3).

2.3. Results and discussion

2.3.1. Tensile tests

The uni-axial stress-strain diagrams of the adhesive Araldite 2015 specimen exhibit a non-linear variation (Figure 7(a)). As the loading rate is increased from 1 to 50 mm/min the stress levels increase regularly. The corresponding strain levels decrease slightly until a loading rate of 30 mm/min and remains same (Table 1). Increasing the loading rate results in roughly an increase of 33% in the failure force levels and a decrease of 14% in the failure displacement levels. Similarly, an increase of 32% in the failure stresses and a decrease of 11% in the failure strains occur. The strain-hardening effect appears on the stress levels; the adhesive strength increases slightly, but the plastic deformation capability of adhesive reduces (Table 1). After a loading rate of 30 mm/min the effect of the loading rate on the stress levels becomes negligible.

PLA specimens were produced in two different forms so that the line of action of the applied tensile load coincides with the raster orientation and layer-build direction, respectively. The uni-axial stress-strain diagrams (Figure 7(b,c)) show that PLA specimens have different non-linear stress-strain variations in both raster orientation and layer-build direction. PLA specimens exhibit higher (1.5 times) failure stress values in the raster orientation as the loading rate is increased. The failure strain (plastic deformation capability) increases negligibly in both directions (Table 1). However, the failure stress increases with increasing loading rate for PLA specimens loaded in raster orientation and in layer-build direction. A higher strength and plastic deformation capability along the raster direction appear. Increasing the loading rate improves strength but plastic deformation capability slightly in both directions. In the layer build direction

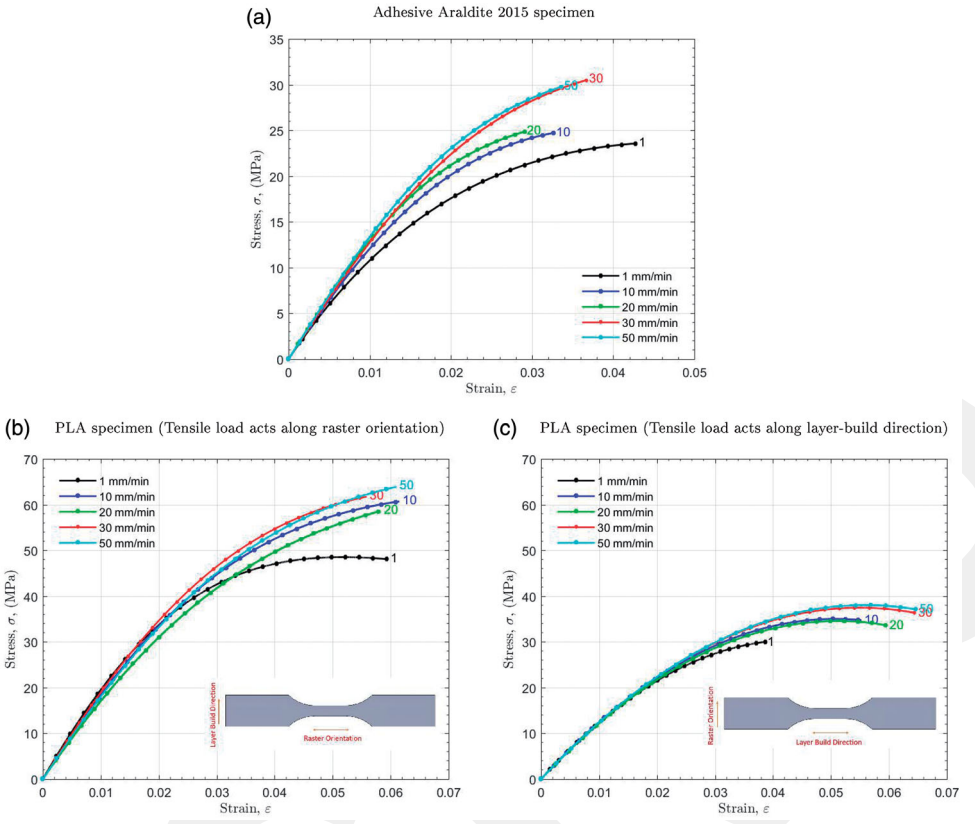

Figure 7. Uniaxial stress-strain diagrams of (a) adhesive Araldite 2015 specimen and (b,c) PLA specimen from the tensile tests at different loading rates.

the filaments are aligned by overlapping and the interfaces between neighbours filaments exhibit a weaker link while the filaments in the raster direction can withstand an axial tensile load by stretching.

Figure 8(a) shows the fractured cross sections of adhesive specimens tested at different loading rates. Adhesive fracture surfaces are very similar and reflect a ductile (elasto-plastic) fracture. Adhesive fails macroscopically by leaving a blank fracture surface with small white spots which are interpreted as extending adhesive residues normal to the fracture surface. An effect of the loading rate is not observed on the fracture surfaces. Figure 8(b,c) also show the fractured cross sections of PLA specimens tested in the layer-build direction and in the raster orientation at different loading rates, respectively. Fracture surfaces of the PLA-specimens from the tensile tests in the layer-build direction are similar and a ductile (elasto-plastic) fracture occurs macroscopically along the interfaces between filament layers (Figure 8(b)). The deformed dark black spots are voids between filaments due to the 3D-printing manufacturing technique. In fact, they have nearly circular geometry in original specimen, but their deformed geometries indicate a considerable axial stretching as well as necking through the specimen section. These voids can not transfer internal load to neighbouring regions. However,

Table 1. Tensile test results of adhesive Araldite 2015 and PLA.

	Modulus of elasticity, GPa	Loading rate mm/min	Failure stress MPa	Std	Failure strain mm/mm (%)	Std (%)	Failure load N	Std	Failure displacement mm	Std
Adhesive	1.32 ± 0.1	1	21.89	2.02	4.1	0.3	202	19	2.0	0.2
		10	23.96	0.55	3.0	0.3	221	5	1.5	0.1
		20	22.61	1.20	2.6	0.3	209	11	1.3	0.2
		30	29.05	1.79	3.5	0.3	268	17	1.8	0.1
		50	27.92	0.77	3.3	0.1	258	7	1.6	0.1
PLA – Raster Orientation	2.33 ± 0.2	1	42.00	10.71	5.6	0.6	267	68	1.4	0.2
		10	46.91	12.14	5.0	0.7	298	77	1.3	0.2
		20	53.43	5.59	5.6	0.2	340	36	1.4	0.1
		30	50.36	13.07	5.6	0.1	320	83	1.4	0.1
		50	58.86	3.57	5.9	0.3	374	23	1.5	0.1
PLA – Layer build direction	1.96 ± 0.1	1	27.59	8.09	3.8	0.3	176	52	0.9	0.1
		10	39.43	3.16	5.3	0.8	251	20	1.3	0.2
		20	41.31	2.00	4.2	0.5	263	12	1.1	0.1
		30	45.13	2.32	4.8	0.7	287	15	1.2	0.2
		50	39.74	3.39	4.2	0.3	253	22	1.1	0.1

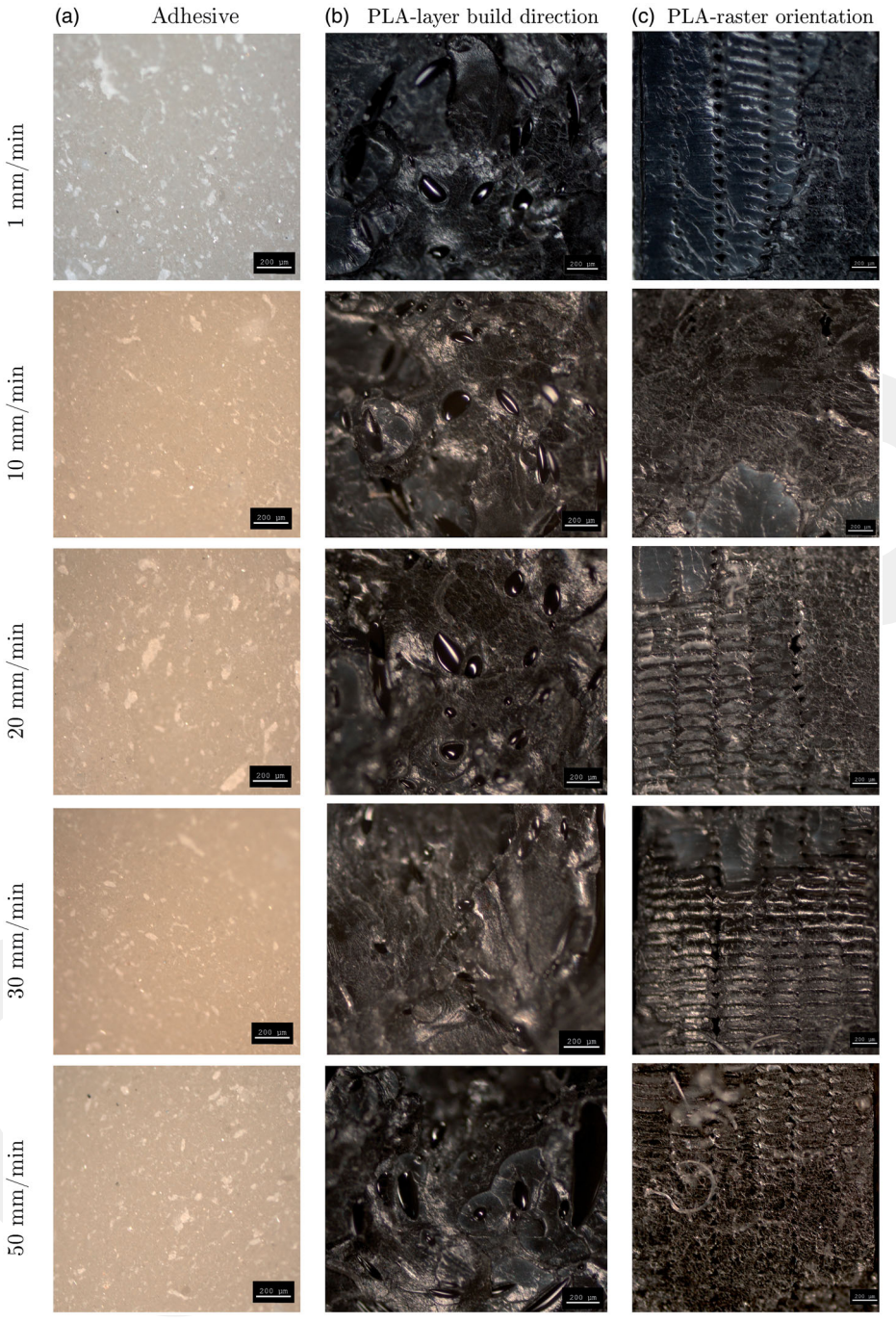

Figure 8. Photographs of fracture surfaces of adhesive, 3D-printed PLA specimens in (b) layer build direction, and (c) in raster orientation after tensile tests at different loading rates.

the solid filament regions carry internal loads and their bright local fracture surfaces indicate a ductile (elasto-plastic) fracture in shear. As the loading rate is increased the deformed geometries of voids between filaments become apparent. In the raster orientation (Figure 8(c)), the filaments are parallel to the action-line of the applied tensile load. The 3D-printing achieves a good bonding between the columns of filaments. The original geometry of these voids is not distorted apparently in the middle regions of the specimen cross sections; this shows that the lateral contraction is more affective on the voids near the free lateral surfaces of specimens. The internal load is transferred through the filaments, and a ductile fracture occurs through the filament sections. As the loading rate is increased the effect of the lateral contraction becomes apparent on the deformed geometry of voids.

For the tensile test specimens of the adhesive single-lap joint (Figure 4) the upper and lower PLA adherends were bonded in the raster orientation coinciding with the direction of the applied axial tensile load since PLA adherends have higher strength in raster orientation. Two PLA tabs of 25×25 mm, which have the same raster orientation as the upper and lower PLA adherends, were bonded to the clamping ends of two adherends so that the line of action of applied tensile load can pass through the centroid of the cross-section of adhesive layer (Figures 4 and 5(a)). Thus, the applied tensile load (P) is transmitted along each line of action which passes through the centroid of the cross section of each adherend due to joint geometry (Figure 9(a)), this eccentricity (e) results in a bending moment, $M = Pe$, in the overlap region where t is adherend thickness (Figure 9(b)). As the overlap region rotates this bending moment increases; therefore, the peeling stresses become apparent around the free edges of adhesive layer [2–4]. Bigwood and Crocombe [42] evaluated this issue in a full elastic analysis of an adherend-adhesive sandwich subjected to any combination of tensile, shear and moment loading being applied at the ends of both adherends, and proposed a simplified formulae which can accurately describe the peak stresses at the ends of the adhesive overlap in both the transverse and longitudinal shear direction. These stresses play an important role in the strength of adhesively bonded single-lap joints although the adhesive joints are designed so that they can withstand shear stresses. The tensile tests of adhesively bonded 3D-printed single-lap joints were repeated five times for each of the loading rates of 1, 10, 20 and 50 mm/min (Figure 5(a)). Table 2 shows for various loading rates the measured failure loads (P_f) and displacements (δ_f) and their averaged values, standard deviations, averaged adhesive shear strength:

$$\tau_a = \frac{P_f}{bl} \tag{4}$$

where b and l are overlap length and width, respectively.

The axial load versus axial displacement variations of 3D-printed PLA adhesive single-lap joint are also plotted in Figure 10. One averaged curve of five test data was considered for each loading rate. The axial load-displacement variations are almost proportional for all loading rates. The failure load and displacement increase with increasing loading rate. The effect of loading rate is more apparent for lower loading rates, such as 1–20 mm/min (Table 2). The strength of adhesively bonded PLA single lap joint is not of apparent sensitivity to loading rate in tension since PLA adherend

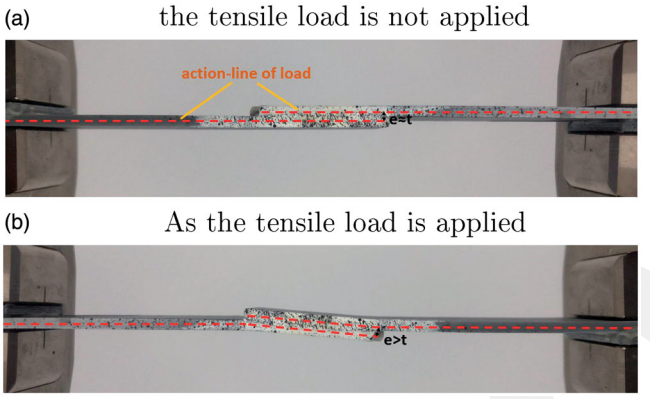

Figure 9. Eccentricity of 3D-printed PLA adhesive single-lap joint in tension.

Table 2. Averaged failure load P_f, displacement δ_f and adhesive shear strength τ_a values of 3D-printed PLA adhesive single-lap joint at different loading rates (Tensile test).

Loading rate	Failure load		Failure		Adhesive
mm/min	P_f (N)	Std.	Displacement δ_f (mm)	Std.	Shear strength τ_a (MPa)
1	1774	204	2.9	0.4	2.44–3.23
10	2570	121	3.8	0.4	3.82–4.33
20	2033	90	3.4	0.5	3.05–3.38
50	2497	197	3.9	0.3	3.48–4.24

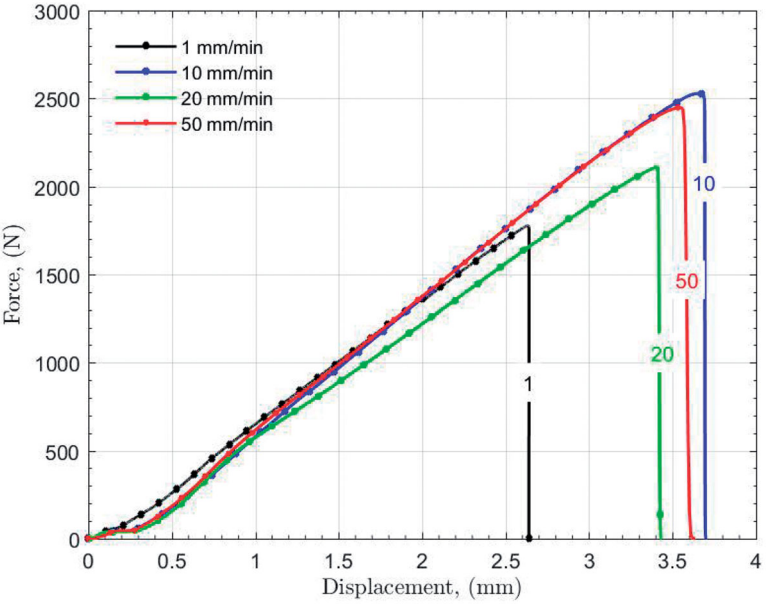

Figure 10. Axial load-displacement diagrams of 3D-printed PLA adhesive single-lap joint from the tensile tests at different loading rates.

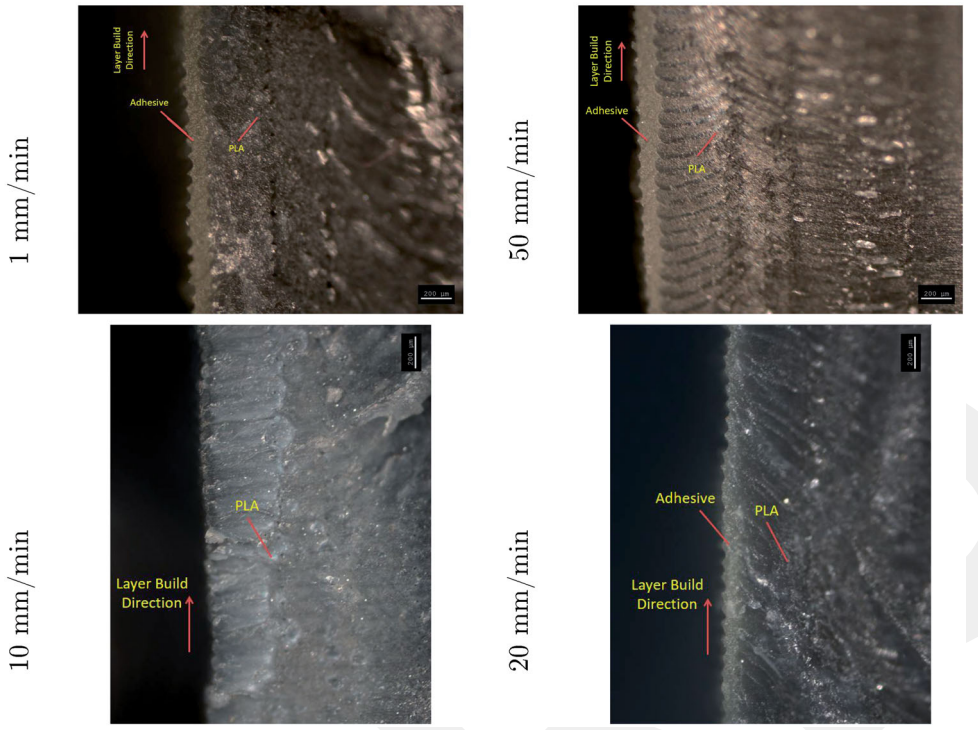

Figure 11. Photographs in the vicinity of the adhesive free edges of 3D-printed PLA adhesive single-lap joints after tensile tests at different loading rates.

has a lower strength in the layer build direction and PLA adherends tend to fail through adherend cross-section in this direction due to the rotation induced by the bending moment. However, the adhesive layer can withstand peeling stresses more than PLA adherends around stress concentration regions.

The photographs of adhesive-adherend interfaces in the failed specimens (Figure 11) show that the adhesive layer interacts with the curved surfaces (filament layers) of PLA adherends which increase bonding area between adhesive and PLA adherends. In case the damage types in each of PLA adherends and adhesive layer are concerned, a small amount of adhesive damage and substantial adherend failure appeared at the loading rates of 1 and 10 mm/min. The damage occurred dominantly in the adhesive layer for 20 mm/min. Both adherend and adhesive damages were observed for 50 mm/min. As the loading rate is increased the failure stresses of both adhesive and PLA adherends in raster orientation increase whereas the failure strains remain almost similar (Figure 7), and the adhesive joint can withstand a higher axial tensile load. The stress concentrations around the free edges of both adhesive-adherend interfaces are the main reason of adherend failure which is initiating at these locations and propagates through the cross section of PLA adherend. In the vicinities of adhesive-PLA adherend interfaces along the joint width around the failure edge after tensile test the colour change in the regions of PLA adherend near the adhesive layer indicates that the shear and extensional deformations varied gradually through the PLA adherend thickness, and becomes more apparent in the vicinities of the adhesive layer (Figure 11). PLA

adherends are more eligible for failure in layer build direction at these loading rates in comparison to adhesive layer.

Figure 12 shows the fracture surfaces of the 3D-printed PLA adhesive single-lap joints after the tensile tests. In order to distinguish specimens for each test the adherends were produced from same PLA material in grey and red colours for tensile test and both bending tests, respectively. The failure appears in both PLA adherend and adhesive layer (Figure 12) for all loading rates. The failure initiates at the free edge of the top adherend-adhesive interface due to stress concentrations and propagates in a small distance along this interface, and a sudden adherend failure occurs (Figures 12 and 13). As the loading rate is increased this damage mechanism is still valid, but the damage in both adherend and adhesive spreads over a larger region. PLA adherend is of a higher strength along the raster orientation than that in the layer-build direction. The adhesive layer exhibits a lower strength in both longitudinal and transverse directions than PLA adherend. Consequently, the first failure initiates in the adhesive layer at the free edge of the adherend-adhesive interface, propagates along this interface at earlier loading stages. However, the damage initiates in the layer build direction in the PLA adherend, and propagates fast along this direction, and the PLA adherend undergoes a sudden failure since it has a lower strength in transverse direction (the layer build direction of PLA adherend) of the adhesive joint. A higher loading rate may result in the adhesive and PLA adherends to gain a better axial strength due to strain hardening. The rotation of overlap region reduces with increasing loading rate (DIC results) and shear effect around the free edges of adhesive layer becomes apparent. As the adhesive layer experiences lower peeling stresses PLA-adherend exhibits sensitivity both shear and bending moment through their cross sections (in the layer build direction) around the free edges of adhesive layer. Thus, the initiation and propagation in the adherend in this direction reduce fast the bending stiffness of PLA-adherend. The completeness of adhesive also helps the bending strength of the PLA adherend in the layer build direction. Finally, PLA adherends can not tolerate this rotations due to their low strength in transverse direction, and fail in the layer build direction around the adhesive free-edges.

2.3.2. Three-point and four-point bending tests

In order to investigate the effect of loading rate on the bending strength with shear of adhesively bonded single-lap joints the three-point bending test was performed five times for each of the loading rates of 1, 10, 30, 50 mm/min, respectively. Table 3 shows the failure loads P_f and the failure cross-head displacements δ_f with standard deviations for different loading rates. Based on the averaged failure loads P_f and cross-head displacements δ_f the maximum bending moment $M_{\max}$ and the bending moment M_{edge} at the free edges of the overlap region were calculated using equations (1-2) for each loading rate (Table 3). The failure load and cross-head displacement increase regularly with increasing loading rate until a loading rate of 30 mm/min and then remain almost same. Consequently, the maximum bending moment $M_{\max}$ and the bending moment M_{edge} at the free edges of the overlap region also increase. This indicates that the strain hardening behaviour of both PLA and adhesive materials improves the overall bending strength with shear of adhesive single-lap joint. Thus, a higher joint failure strength

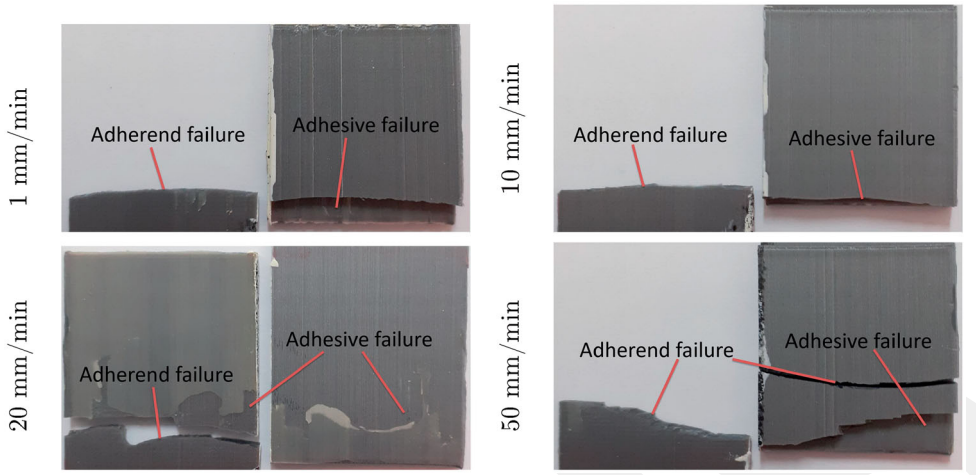

Figure 12. Fracture surfaces of 3D-printed PLA adhesive single-lap joints after tensile tests at different loading rates.

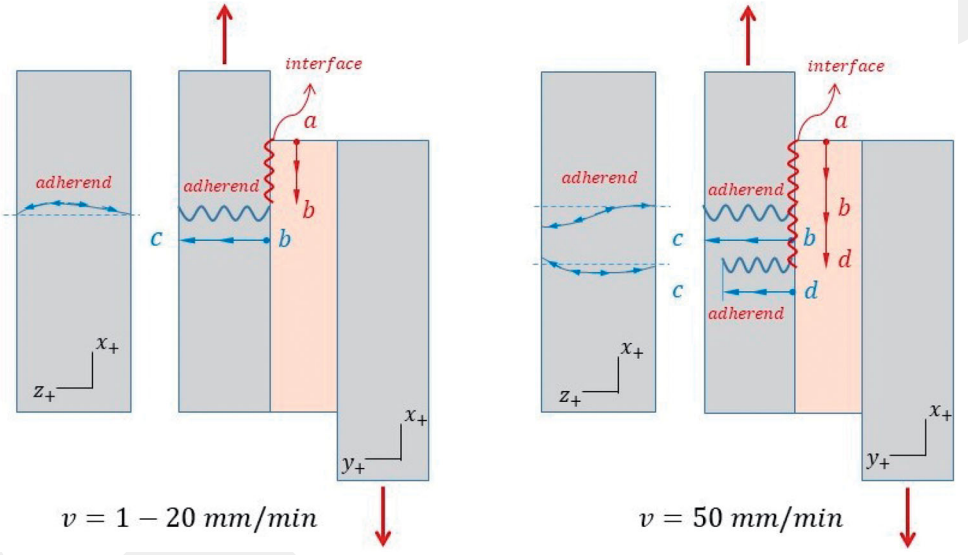

Figure 13. Stages of failure initiation and propagation in adhesive and adherends during the tensile tests of 3D-printed PLA adhesive single-lap joints at different loading rates.

appears since a higher bending moment is required to initiate the adhesive failure and adherend failure in the layer build direction of PLA adherend at the free edges of the adhesive-adherend interfaces.

Figure 14 shows the applied load and cross-head displacement variations for the three-point bending tests at the loading rates of 1, 10, 30, 50 mm/min, respectively. The load-displacement curves vary almost linearly until a specific load or displacement value and then a non-linear large plateau in the curves is observed, finally the adhesive single-lap joint undergoes a sudden failure. Increasing the loading rate results in an increase in both the load and displacement levels. However, this effect becomes small

Table 3. Main results from the three-point bending tests of 3D-printed PLA adhesive single-lap joint at different loading rates.

Loading rate mm/min	Failure load P_f (N)	Std.	Failure disp. δ_f (mm)	Std.	M_{max} N-mm	M_{edge} N-mm
1	37	4	12.4	1.6	924.5	693.4
10	47	3	14.9	1.6	1173.0	879.8
30	51	7	14.9	2.0	1278.8	959.1
50	51	4	15.1	2.6	1264.0	948.0

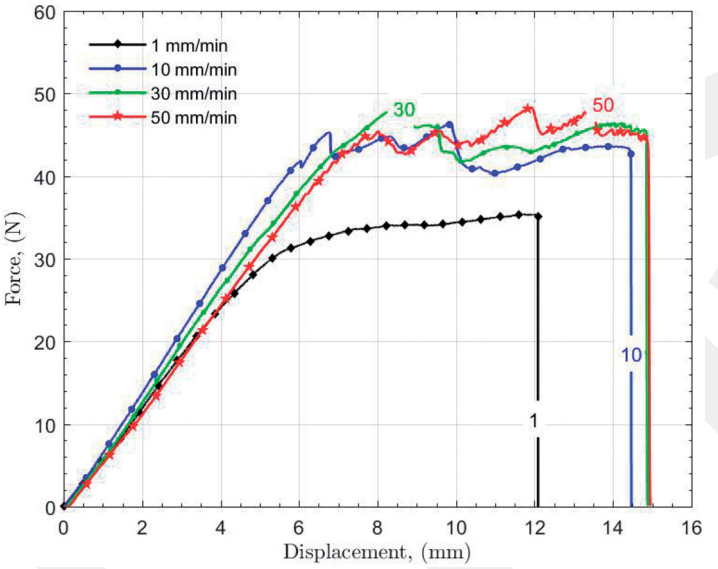

Figure 14. Load-displacement diagrams of 3D-printed PLA adhesive single-lap joint from three-point bending tests at different loading rates.

after a loading rate of 10 mm/min. The strain-hardening capability of both PLA adherends and adhesive layer improves the overall bending strength of adhesive single-lap joint and results in the adhesive joint to withstand a larger load level with increasing loading rate. Thus, a higher failure load and bending moment are required to initiate the adhesive failure at the free edges of the adhesive layer. The shear and peeling stresses concentrate on the free edges of the adhesive layer, the bending moment creates normal stresses in the raster orientation, which vary linearly through the cross section of the PLA adherend whereas the shear stresses act on the cross section of PLA adherends in the layer build direction. Therefore, PLA adherends are stronger in the raster orientation, and can withstand safely normal stresses. The adhesive layer undergoes peak peeling and shear stresses around adhesive free edges and decrease towards the middle of the overlap region, and the peeling stresses cause the adhesive layer with lower strength to be more prone to failure than PLA adherends with higher strength.

In the three-point bending tests adhesively bonded 3D-printed single-lap joints failed along the adhesive-PLA adherend interface, the damages of PLA adherends are not apparent for all loading rates (Figure 15). The failure initiated at the free edge of

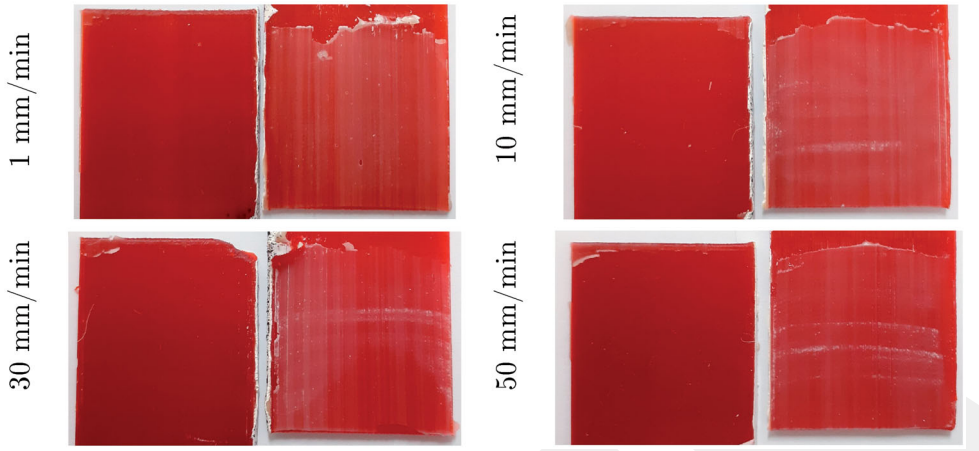

Figure 15. Fracture surfaces of 3D-printed PLA adhesive single-lap joints after three-point bending tests at different loading rates.

Table 4. Main results from the four-point bending tests of 3D-printed PLA adhesive single-lap joint at different loading rates.

Loading rate mm/min	Failure load P_f (N)	Std.	Failure disp. δ_f (mm)	Std.	$M_{max}=M_{edge}$ N-mm
1	96	6	22.4	3.7	1194.4
10	85	3	14.2	3.7	1065.3
30	88	4	15.5	1.9	1103.4
50	87	4	15.1	2.5	1083.5

the top adherend-adhesive interface and propagated along this interface for all loading rates. As the loading rate is increased, the adhesive failure surfaces exhibit a wavy propagation. Thus, as the loading rate is increased the deformation energy is restored and released with the failure of remaining adhesive layer in a shorter duration. In addition, the failure propagates fast in the middle of bonding region whilst it propagates at a lower speed along both side edges of bonding region as a result of lateral contraction due to Poisson's effect. As the damage propagates both peeling and shear stresses increase at the free edges of the adhesive bonding region. The adherends are forced to deform plastically and their deformed geometries change relatively as the damage propagates. This affects negatively the stress and strain states around the adhesive free edges.

The four-point bending tests without shear were repeated five times for each of the loading rates of 1, 10, 30, 50 mm/min, respectively. Table 4 shows the averaged failure loads P_f and the failure cross-head displacements δ_f for various loading rates. The failure load and cross-head displacement decrease regularly with increasing loading rate, but they change negligibly after a loading rate of 10 mm/min. The bending moment M_{edge} at the free edges of the overlap region was calculated using Equation (3) for each loading rate (Table 4). As the loading rate is increased, this bending moment at edges decreases at failure.

Figure 16 shows the averaged applied load and cross-head displacement variations for the four-point bending tests at the loading rates of 1, 10, 30, 50 mm/min,

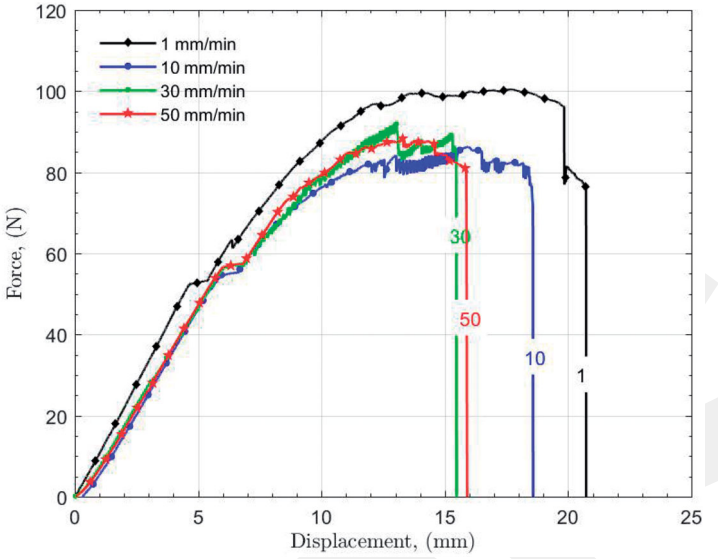

Figure 16. Load-displacement diagrams of 3D-printed PLA adhesive single-lap joint from four-point bending tests at different loading rates.

respectively. The load-displacement curves vary almost linearly until a specific load or displacement value which indicates the plastic deformation initiation and propagation in both adhesive and PLA adherends. As a result, an apparent non-linear variation in the load-displacement curves appears, finally the adhesive single-lap joint experiences a sudden failure. Increasing the loading rate results in a decrease in both the load and displacement levels. However, this effect becomes negligible after a loading rate of 10 mm/min. The peeling stresses become more effective around the free edges of the adhesive layer since the shear force is zero and bending moment remains constant in the overlap region. As the loading rate is increased the joint failure occurs at lower cross-head displacements. The four-point bending tests show that the adhesively bonded PLA single lap joints lose their load carrying capability since the peeling stresses around the adhesive free edges reach earlier to failure levels with increasing loading rate.

The failure initiates at the free edge of the adherend-adhesive interface and propagates along this interface for all loading rates (Figure 17). As the loading rate is increased, a clean separation is observed along this interface contrary to the wavy fracture surfaces in the three-point bending tests. The fracture surface of the upper adherend is exposed. The peeling stresses around the adhesive free edges are main reason of this interfacial failure which occurs widely in the joint. The failure propagates fast in the middle of overlap region in comparison with those near the side edges of the overlap region due to Poisson's effect, but this mechanism becomes negligible for higher loading rates of 30 and 50 mm/min.

2.3.3. Strain distributions via digital image correlation (DIC) method

The 3D-printed adhesive single-lap joint can present a good load carrying capability in tension and under bending moment with/without shear. The failure of adhesive joint

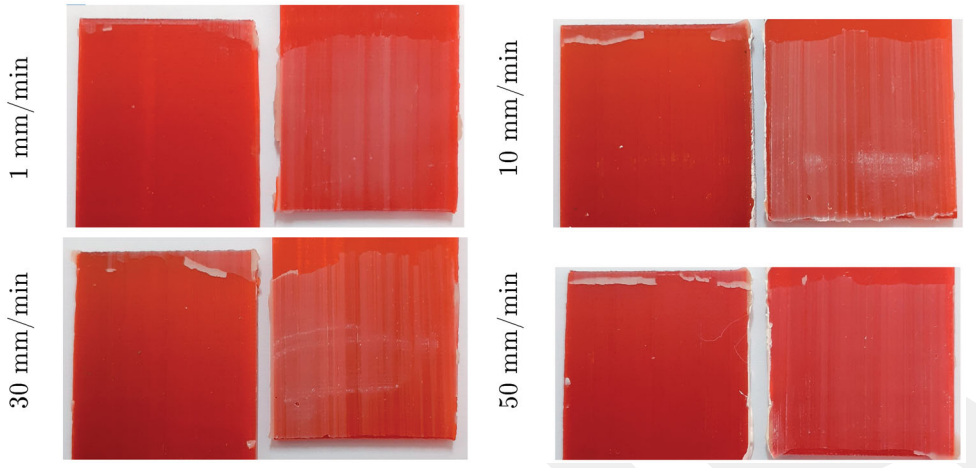

Figure 17. Fracture surfaces of 3D-printed PLA adhesive single-lap joints after four-point bending tests at different loading rates.

in tensile loading initiated at the free edge of top adherend-adhesive interface, and propagated in a small distance along this interface, and then failed completely between the filament layers through the thickness of top adherend (Figure 12). For tensile loading the failure initiation is mainly due to the stress concentrations occurring around the free edges of adhesive layer.

In order to determine the strain concentration regions and the probable location of the first failure in the adhesive single-lap joint in tension the displacement fields were measured by means of Digital Image Correlation (DIC) Method [43]. This method is very useful to see the displacement and strain fields on set of the joint failure. However, the method is successful for only small displacements and rotations. Following the production of the 3D-printed PLA adhesive single-lap joints, the front face was painted first in white colour, and then a black paint was sprayed on this surface to form speckled patterns (Figure 5). DIC method uses the images (deformed geometry) of the painted face of the adhesive joint framed at a suitable interval as the load is applied and compares them with the original (undeformed) image of this face using various algorithms. DIC image processing and the calculation of strain distributions were carried out using an open source 2D Digital Image Correlation MATLAB code, Ncorr [44]. A number of studies has verified its performance and accuracy with both experimental data and other commercial softwares, and stated that Ncorr software was capable of determining the displacement and strain distributions [45,46].

Since the three-point and four-point bending tests resulted in large displacements and rotations, the displacement fields were not measured and calculated accurately. For this reason DIC method was applied to only the tensile test of 3D-printed PLA adhesive single-lap joints. The painted front face of overlap region was recorded by a digital camera having a high resolution 4 K video. Then, this recorded video was divided into a certain number of frames and instant photographs. Each member of speckle family on the painted front face of the overlap region was traced by Ncorr software, and the displacement components of each member were calculated by comparing its original

location, first the spatial derivatives of the displacement components and then the strain components were calculated for each member based on the small strain-small displacement theory of the elasticity. The frames were taken at the cross-head displacements δ of 2.63, 3.66, 3.41 and 3.55 mm (on set of the failure as possible) for the loading rates of 1, 10, 20 and 50 mm/min, respectively. The displacement and strain distributions were calculated from the tensile test of the first specimen of each specimen group for each loading rate.

Figure 18 shows the calculated transverse strain ε_{xx}, longitudinal strain ε_{yy}, and shear strain ε_{xy} distributions on set of the joint failure as possible. The transverse (peeling) strain ε_{xx} concentrates around the free edges of the top and bottom adherend-adhesive interfaces for loading rates of 1 and 10 mm/min. The transverse strain spreads through-the-thickness of the top adherend near the free edge of the top adherend-adhesive interface, and becomes more critical for the top adherend failure. The adhesive failure initiates and propagates through the adhesive interface for higher loading rates, and then adherend failure occurs. Similarly, the longitudinal strain ε_{yy} concentrates around the free edges of the top and bottom adherend-adhesive interfaces for all loading rates, and penetrates apparently through-thickness of the neighbour adherend, and contributes a probable adherend failure. The longitudinal strain levels increases considerably with increasing loading rate. The shear strain ε_{xy} concentrated around the free edges of the adhesive layer is critical as much as the longitudinal strain, and increases with increasing loading rate. DIC analysis shows that the 3D-printed PLA adhesive single-lap joint experiences strain concentrations around the adhesive free edges in a tensile load. In particular the longitudinal and shear strain distributions become more effective along the through-thickness of the load-transmitting adherend and the joint failure occurs through the thickness of this PLA adherend.

Based on DIC analysis the peak normal strains ε_{xx} are between 1.5 and 6.0%, the normal strains ε_{yy} are between 3.5 and 6.0%, and the shear strains ε_{xy} are between 2.5 and 5.0%, respectively. The PLA specimens in tensile tests failed at failure strains in range of 5.0–5.9% in the raster orientation and at failure strains in range of 3.8 and 5.3% in the layer-build direction, respectively (Table 1). The adhesive specimens in tensile test failed at strain values in range of 2.6–4.1% for different loading rates of 1–50 mm/s (Table 1). These failure strain values are not affected evidently at loading of rates above 10 mm/s, it becomes stable between 2.6 and 3.5%.

The uniaxial tensile tests at different loading rates can give information about only one dimensional mechanical behaviour of PLA and adhesive specimens. The DIC method is able to give information accurately about their two-dimensional strain states. Therefore, the strain distributions calculated using the DIC method, especially in the strain concentration regions are reasonably acceptable. A quadratic two-dimensional failure criterion based on an equivalent strain in terms of normal and shear strain components would be useful for the comparison of the failure strain obtained from the uniaxial tensile tests with the equivalent strain value for both adhesive and PLA materials, such as von Mises criteria for a ductile material as follows

$$\varepsilon_{eqv} = \frac{\sqrt{2}}{2}\sqrt{(\varepsilon_1 - \varepsilon_2)^2 + (\varepsilon_2 - \varepsilon_3)^2 + (\varepsilon_3 - \varepsilon_1)^2} \tag{5}$$

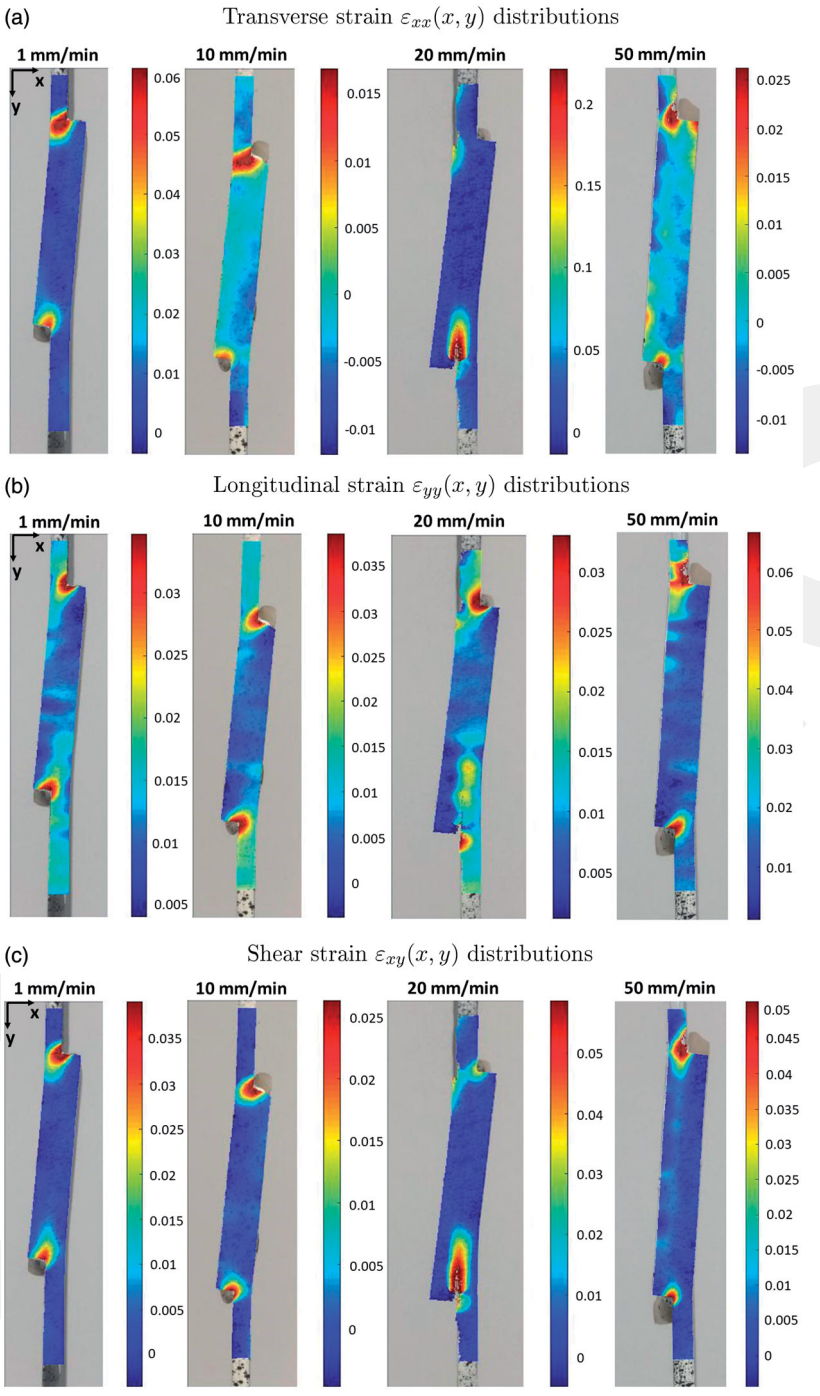

Figure 18. (a) Transverse strain $\varepsilon_{xx}(x, y)$, (b) longitudinal strain $\varepsilon_{yy}(x, y)$ and (c) shear strain $\varepsilon_{xy}(x, y)$ distributions in the overlap region on set of failure for the tensile test.

Table 5. Failure strains ε_f measured from the tensile tests and peak equivalent strains ε_{eqv} calculated from DIC analysis of 3D-printed PLA adhesive single-lap joint in tension at different loading rates.

Failure strains ε_f (%) (Table 1)					Equivalent strains ε_{eqv} (%) (DIC)				
	Loading rate (mm/min)					Loading rate (mm/min)			
Material	1	10	20	50	Joint member	1	10	20	50
PLA-RO	5.6	5.0	5.6	5.9	Top PLA	7.9	5.2	8.5	10.1
PLA-LBD	3.8	5.3	4.2	4.2	Bottom PLA	7.7	5.2	8.5	9.4
Adhesive	4.1	3.0	2.6	3.3	Adhesive	7.9	5.2	8.5	9.4

where $\varepsilon_1, \varepsilon_2$ and ε_3 are principal strains, respectively. It can be reduced to two-dimensional plain-strain state with $\varepsilon_3 = 0$.

Table 5 compares the equivalent strains calculated from DIC analysis of 3D-printed PLA adhesive single-lap joint in tension at different loading rates with the failure strains obtained from the uniaxial tensile tests of both PLA and adhesive specimens. The peak equivalent strains were considered in strain concentration regions. In vicinity of the bi-material interface the peak strain components were evaluated at the nearest available point on both sides of adhesive and PLA adherends. However, we expect a continuous strain distributions since they calculated from the spatial derivatives of displacement components. The peak equivalent strains were very close in PLA adherends and adhesive in the peak strain points, and were simply calculated as 7.7–7.9, 5.2, 8.5, 9.4–10.1% for the loading rates of 1, 10, 20 and 50 mm/s, respectively. Consequently, this simple calculation indicates that both adhesive layer and PLA adherends in the strain concentration regions underwent failure at these loading stages in case they were compared with their failure strains in tension. PLA adherend having lower through-thickness strength goes failure through the adherend thickness after a damage propagation at a short distance along the adhesive layer from these free edges. The rotation degree of the overlap region also affects strain distributions around the geometrically discontinuous adhesive free edge. As the loading rate is increased the rotation of the overlap region reduces slightly, and the longitudinal strain ε_{yy} and shear strain ε_{xy} components become more effective whilst the transverse (peeling) strain ε_{xx} reduces.

3. Conclusions

This experimental study investigates the applicability of the adhesive bonding technique for PLA adherends produced with additive manufacturing and especially the effects of the loading rate (cross-head speed) on the strength of adhesively bonded 3D-printed PLA single-lap joints under tensile, three-point bending (with shear) and four-point bending (no shear effect) loadings. The main results are as follows:

- Araldite 2015 adhesive exhibits a non-linear force-displacement variation, a higher strength but a decreasing failure strain with increasing loading rate (cross-head speed) in tension. Similarly, PLA specimens exhibit different mechanical behaviour in the raster orientation and layer-build direction, and has a force-displacement

variation with a small non-linearity for each loading rate. Its strength and extension ability in the raster orientation are better than those in the layer-build direction. PLA shows higher strength in the raster orientation and in the layer-build direction than that of adhesive material.

- In tensile tests the adhesive single-lap joints showed almost linear load-displacement variations and a sudden failure. The load bearing capability increased slightly with increasing loading rate due to the strain hardening property of both PLA and adhesive materials. The failure initiated at the free edge of the top adherend-adhesive interface, propagated a small distance along this interface and the top adherend failed suddenly through the adherend (cross-section) thickness since the large rotations occur in the overlap region and PLA adherend was of a lower strength along the layer-build direction, especially along the interface between filaments.
- In three-point bending tests the load-displacement curves had a linear variation until the failure initiated and then a large increase in displacement occurred versus a small change in the applied load level. The failure initiated at the free edge of the top adherend-adhesive interface, and propagated along this interface in wavy form. The load and displacement increased with increasing loading rate. Similar failure mechanism occurred in four-point bending tests, but an exposed fracture surface appeared on the top adherend. The contribution of shear force to the adhesive damage was apparent in three-point bending test. The damage propagated longitudinally in the middle of overlap region than along the side edges of overlap region due to Poisson's effect.
- The adherend failure occurred through the thickness of PLA adherend at which the load is applied after a failure initiation and propagation in vicinity of the adhesive free edges since PLA adherend was of a lower strength in layer build direction.
- All tensile tests for adhesive, PLA specimens and all tensile and bending tests of adhesive PLA single lap joints indicated that the load-force and stress-strain variations exhibit small sensitivity to the range of present loading rate.

Disclosure statement

No potential conflict of interest was reported by the author(s).

ORCID

M. Kemal Apalak http://orcid.org/0000-0002-3263-5735

References

[1] Gibson I, Rosen D, Stucker B. Additive manufacturing technologies: 3D printing, rapid prototyping, and direct digital manufacturing. 2nd ed. New York: Springer; 2015.
[2] Adams RD, Comyn J, Wake WC. Structural adhesive joints in engineering. London, UK: Chapman & Hall; 1997.
[3] Kinloch AJ. Adhesion and adhesives: science and technology. Netherlands: Springer Science & Business Media; 2012.

[4] Grant LDR, Adams RD, da Silva LFM. Experimental and numerical analysis of single-lap joints for the automotive industry. Int J Adhes Adhes. 2009;29(4):405–413.
[5] Esmaeili E, Razavi SMJ, Bayat M, et al. Flexural behavior of metallic fiber-reinforced adhesively bonded single lap joints. J Adhes. 2018;94(6):453–472.
[6] Karachalios EF, Adams RD, da Silva LFM. The behaviour of single lap joints under bending loading. J Adhes Sci Technol. 2013;27(16):1811–1827.
[7] Malvade I, Deb A, Biswas P, et al. Numerical prediction of load–displacement behaviors of adhesively bonded joints at different extension rates and temperatures. Comput Mater Sci. 2009;44(4):1208–1217.
[8] Blackman BRK, Kinloch AJ, Rodriguez-Sanchez FS, et al. The fracture behaviour of adhesively-bonded composite joints: Effects of rate of test and mode of loading. Int J Solids Struct. 2012;49(13):1434–1452.
[9] Al-Zubaidy HA, Zhao XL, Al-Mahaidi R. Experimental evaluation of the dynamic bond strength between CFRP sheets and steel under direct tensile loads. Int J Adhes Adhes. 2013;40:89–102.
[10] Al-Zubaidy HA, Zhao XL, Al-Mahaidi R. Mechanical characterisation of the dynamic tensile properties of CFRP sheet and adhesive at medium strain rates. Compos Struct. 2013;96:153–164.
[11] Murakami S, Sekiguchi Y, Sato C, et al. Strength of cylindrical butt joints bonded with epoxy adhesives under combined static or high-rate loading. Int J Adhes Adhes. 2016;67:86–93.
[12] Kovan V, Altan G, Topal ES. Effect of layer thickness and print orientation on strength of 3D printed and adhesively bonded single lap joints. J Mech Sci Technol. 2017;31(5):2197–2201.
[13] Garcia R, Prabhakar P. Bond interface design for single lap joints using polymeric additive manufacturing. Compos Struct. 2017;176:547–555.
[14] Spaggiari A, Denti F. Mechanical strength of adhesively bonded joints using polymeric additive manufacturing. Proc Inst Mech Eng Part C J Mech Eng Sci. 2019;:095440621985022.
[15] Bürenhaus F, Moritzer E, Hirsch A. Adhesive bonding of FDM-manufactured parts made of ULTEM 9085 considering surface treatment, surface structure, and joint design. Weld World. 2019;63(6):1819–1832.
[16] Caminero MA, Chacón JM, García-Moreno I, et al. Interlaminar bonding performance of 3D printed continuous fibre reinforced thermoplastic composites using fused deposition modelling. Polym Test. 2018;68:415–423.
[17] Leicht H, Orf L, Hesselbach J, et al. Adhesive bonding of 3D-printed plastic components. J Adhes. 2019;:1–16.
[18] Yap YL, Toh W, Koneru R, et al. Evaluation of structural epoxy and cyanoacrylate adhesives on jointed 3D printed polymeric materials. Int J Adhes Adhes. 2020;100:102602.
[19] ASTM D638-14 standard test method for tensile properties of plastics; 2014. https://www.astm.org/Standards/D638.
[20] Ayatollahi MR, Nabavi-Kivi A, Bahrami B, et al. The influence of in-plane raster angle on tensile and fracture strengths of 3D-printed PLA specimens. Eng Fract Mech. 2020;237:107–225.
[21] Caminero MÁ, Chacón JM, García-Plaza E, et al. Additive manufacturing of PLA-based composites using fused filament fabrication: Effect of graphene nanoplatelet reinforcement on mechanical properties, dimensional accuracy and texture. Polymers. 2019;11(5):799.
[22] Ferreira RTL, Amatte IC, Dutra TA, et al. Experimental characterization and micrography of 3D printed PLA and PLA reinforced with short carbon fibers. Compos Part B-Eng. 2017;124:88–100.
[23] ISO 527-2 plastics—determination of tensile properties – part 2: test conditions for moulding and extrusion plastics. 2012. https://www.iso.org/standard/56046.

[24] SOLIDWORKS 3D Design Software – Dassault Systèmes, https://www.3ds.com.
[25] Ultimaker Cura: Powerful, easy-to-use 3D printing software, https://ultimaker.com/.software/ultimaker-cura.
[26] Jennings CW. Surface roughness and bond strength of adhesives. J Adhes. 1972;4(1):25–38.
[27] Harris AF, Beevers A. The effects of grit-blasting on surface properties for adhesion. Int J Adhes Adhes. 1999;19(6):445–452.
[28] Spaggiari A, Dragoni E. Effect of mechanical surface treatment on the static strength of adhesive lap joints. J Adhes. 2013;89(9):677–696.
[29] ASTM D5868 – 01 Standard test method for lap shear adhesion for fiber reinforced plastic (FRP) bonding; 2014. https://www.astm.org/Standards/D5868.
[30] ASTM D5573 - 99 Standard practice for classifying failure modes in fiber-reinforced-plastic (FRP) joints; 2019. https://www.astm.org/Standards/D5573.
[31] Gleich DM, Tooren MJL, Van Beukers A. Analysis and evaluation of bondline thickness effects on failure load in adhesively bonded structures. J Adhes Sci Technol. 2001;15(9):1091–1101.
[32] Kawashita LF, Kinloch AJ, Moore DR, et al. The influence of bond line thickness and peel arm thickness on adhesive fracture toughness of rubber toughened epoxy – aluminium alloy laminates. Int J Adhes Adhes. 2008;28(4-5):199–210.
[33] Castagnetti D, Spaggiari A, Dragoni E. Effect of bondline thickness on the static strength of structural adhesives under nearly-homogeneous shear stresses. J Adhes. 2011;87(7–8):780–803.
[34] Akhavan-Safar A, Ayatollahi MR, da Silva LFM. Strength prediction of adhesively bonded single lap joints with different bondline thicknesses: a critical longitudinal strain approach. Int J Solids Struct. 2017;109:189–198.
[35] Machado JJM, Marques EAS, Silva MRG, et al. Numerical study of impact behaviour of mixed adhesive single lap joints for the automotive industry. Int J Adhes Adhes. 2018;84:92–100.
[36] Nakamura N, Mori K, Abe F, et al. Bending of sheet metals using plastic tools made with 3D printer. Procedia Manuf. 2018;15:737–742.
[37] Zaragoza VG, Strano M, Iorio L, et al. Sheet metal bending with flexible tools. Procedia Manuf. 2019;29:232–239.
[38] Nakamura N, Mori K, Abe Y. Applicability of plastic tools additively manufactured by fused deposition modelling for sheet metal forming. Int J Adv Manuf Technol. 2020;108(4):975–985.
[39] Mercado-Colmenero JM, Rubio-Paramio MA, la Rubia-Garcia MD, et al. A numerical and experimental study of the compression uniaxial properties of PLA manufactured with FDM technology based on product specifications. Int J Adv Manuf Technol. 2019;103(5–8):1893–1909.
[40] ASTM D790-17 Standard test methods for flexural properties of unreinforced and reinforced plastics and electrical insulating materials; 2017. https://www.astm.org/Standards/D790.
[41] ASTM D6272-17 Standard test method for flexural properties of unreinforced and reinforced plastics and electrical insulating materials by four-point bending; 2017. https://www.astm.org/Standards/D6272.
[42] Bigwood DA, Crocombe AD. Elastic analysis and engineering design formulae for bonded joints. Int J Adhes Adhes. 1989;9(4):229–242.
[43] Pan B, Xie H, Guo Z, et al. Full-field strain measurement using a two-dimensional Savitzky-Golay digital differentiator in digital image correlation. Opt Eng. 2007;46(3):033601.
[44] Ncorr open-source 2D digital image correlation Matlab Software. http://www.ncorr.com.
[45] Blaber J, Adair B, Antoniou A. Ncorr: open-source 2D digital image correlation matlab software. Exp Mech. 2015;55(6):1105–1122.
[46] Quanjin M, Rejab MRM, Halim Q, et al. Experimental investigation of the tensile test using digital image correlation (DIC) method. Mater Today Proc. 2020;27(2):757–763.